MODELING OF STATIC INDENTATION ON LAMINATED COMPOSITE SHELLS

Kaustav Mitra*, Dineshkumar Harursampath†
Aerospace Engineering Department, Indian Institute of Science
Bangalore, India

Abstract

Current analysis on static indentation predominantly focus on a plate models for simulation of indentation. In this work, we consider the curvature effects that become predominant with the increase in transverse displacement of the plate. The 3-D shell model is employed for simulating indentation to capture the non-linear behaviour due to curvature effects. VAM is applied to reduce the 3-D problem to a 2-D Reissner-Mindlin constitutive form through a 1-D normal line analysis. The resulting 2-D model is solved for unknown contact forces and displacements at each level of indentation. The model is meshed using 4-noded degenerate quadrilateral elements with shape functions defined by the Bernstein basis functions. Power law contact force-indentation relationships have been proposed for symmetric, cross and angle ply lay-ups. Curvature effects on contact force and their dependence on indentation are also analysed. Variation of indentation energy with lay-up angle is also depicted for use in delamination studies. The simulation results were compared with analytical and experimental results for sandwich laminates of different lay-up configuration and they show good agreement with published data.

Nomenclature

A	Shell Stiffness Matrix
A_R	In-plane Shell Stiffness Matrix
B	Strain-Displacement Matrix
B_i	Strain-Displacement Matrix for i-th node
C_1, C_2	Fit Coefficients in Contact Law
E_{indt}	Indentation Energy
F	Force-Material Coupling Vector
F_e	Element Force-Material Coupling Vector
$\overline{F}$	Force-Material Coupling Vector for unit load
$\tilde{F}$	Element Force-Material Coupling Vector
f	Function of Indentor geometry
g_N	Gap function
h	Indentation depth
$\mathbf{J}$	2-D Jacobian Matrix
K_e, K_{ee}	Element Elastic Stiffness Matrix
K_{ce}	Element Displacement-Contact Coupling Matrix
K^a_{ee}	Assembled Element Elastic Stiffness Matrix
K^a_{ce}	Assembled Element Displacement Contact Coupling Matrix
$\mathbf{n}$	Normal Vector at Contact Node
N	Displacement Shape Function Matrix
$\tilde{N}$	Contact Force Shape Function Matrix
N_i	Shape Function for i-th node
q	Transformation Matrix from Lamina Coordinates to Global Cartesian Coordinates
$\underline{q}$	In-plane Transformation Matrix from Lamina Coordinates to Global Coordinates
$\mathbf{R}_i$	Direction cosine Matrix of Lamina Coordinates w.r.t. Local Normal Vector for i-th node
$\underline{\mathbf{R}}_i$	In-plane Direction cosine matrix of Lamina Coordinates w.r.t. Local Normal Vector for i-th node
$\Re$	In-plane Reissner-Mindlin Strain Measures
R_c	Element Residual due to specified Contact Constraints
R^a_c	Assembled Residual for Specified Contact Constraints

*Corresponding Author: *email-id*: kaustav_cal@yahoo.com
†*email-id*: dinesh@aero.iisc.ernet.in

t_i	Shell Thickness at i-th node
t_N	Contact Force
$\overline{t}_N$	Nodal Contact Force
$\mathbf{T}$	Global Vector of Unknown Contact Tractions
(u, v, w)	Displacement Components
U	Vector of Element Displacements
U_e	Vector of Element Nodal Displacements
$\mathbf{U}$	Global Vector of Unknown Displacements
$\mathbf{v}_{3i}$	Normal Vector at i-th node
(x_1, x_2, x_3)	Curvilinear Coordinate System
(x, y, z)	Global Cartesian Coordinate System
$(\underline{x}, \underline{y}, \underline{z})$	Local Cartesian Coordinate System
$\epsilon^*_{\alpha\beta}$	In-plane Reissner-Mindlin Strain Components
(ξ, η, ζ)	Natural Curvilinear Coordinates for Shell Element
$\gamma^*_{\alpha 3}$	Reissner-Mindlin Shear Strains
γ	Shear Strain Vector
Γ	Inverse 2-D Jacobian Matrix
∂	Partial Operator on Displacement Vector
θ_1, θ_2	Rotation of the Normal Vector after Deformation
$\kappa^*_{\alpha\beta}$	In-plane Reissner-Mindlin Curvature Components
Π_e	Element Potential arising out of Contact Constraints
Π_c	Total Energy Potential due to Contact Constraints
$\Pi_{\Re}$	Total Elastic Potential of the Shell Surface
Π_T	Total Constrained Energy Potential of any Shell Element

Introduction

One of the primary requirements to be fulfilled by a primary aeronautical structure made of carbon fiber reinforced plastic (CFRP) is its ability to bear the assigned loads when a realistic distribution of barely visible impact damages (BVID) is present. Although there is no general agreement on the precise meaning of 'barely visible' for an impact damage, the parameter almost universally used to quantify this property is indentation. In practice, when the suitability of an aeronautical component to withstand the design loads must be verified, the dent depth corresponding to a BVID is conventionally assigned, the geometry of an impactor destined to impart the wanted BVID is fixed, and the energy necessary to induce the specified level of damage is experimentally found by trial-and-error, using specimens representative of the actual situation; finally, the information gathered is employed to induce the desired damages in the real component to be tested. This procedure is complicated by the fact that, in general, the dent depth is strongly dependent on many parameters, among which the most relevant are the particular laminate under consideration, its thickness, the constraints, the indentor geometry and the impact speed. Therefore, the availability of analytical tools for prediction of the indentation induced deformations and the estimation of the resulting stress field would greatly help in simplifying the problem.

The problem of static indentation has been dealt with through the help of experiments and is well understood in the literature. Caprino[1] assessed a simple power-law equation correlating the indentation depth with impact energy. It was shown that the ratio of the impactor energy to the penetration energy when adopted as an independent parameter, the relationship proposed is negligibly affected by the laminate type and thickness. On the other hand, the penetration energy was also calculated through a model developed by Caprino *et al* in [2] and [3], accounting only for the reinforcement volume and indentor diameter. Caprino *et al* in [4] performed quasi-static indentation tests on CFRP plates and a new efficient model was proposed indicating that impact tests can be substituted with static tests, when the response of a CFRP laminate in terms of indentation and penetration is under study. Bogdanovich[5] did three dimensional contact-impact analysis on composite laminated beams and plates exposed to rigid body impact. He applied Bernstein basis polynomials for displacement approximation in the three directions for predicting the 3-D transient deformation. Anderson[6] investigated force-indentation response of sandwich panels subjected to a rigid spherical indentor. A three dimensional analytical solution method was used to obtain the complete stress and displacement fields as well as the contact pressure arising from static indentation. Hodges[7] gave analytical solution to a beam or plate being pressed against a flat surface using the variational asymptotic method. However, he only considered isotropic materials and the beams and plates were modelled according to Timoshenko beam theory and Reissner-Mindlin plate theory respectively.

In the above works, the stiffness, laminate properties, lay-up and thickness effects were not taken into account. The analytical studies on static indentation so far have mainly focussed on plate models. They do not address the development of membrane effects, as the plate undergoes transverse displacements and assume the shape

of a shell. This fact motivates us to go for shell models to investigate the influence of curvature induced effects.

The simplest shell theory is the classical lamination theory, which is based on the Kirchhoff hypothesis. However, even for thin composite shells this theory gives very poor results compared to the actual 3-D solution. But it is plausible to take into account the smallness of the thickness of the structures and construct an accurate 2-D model for a 3-D body. The attempts to rationally improve upon the classical model have been based on *ad hoc* kinematic assumptions like an *a priori* distribution of displacement through the thickness, which cannot be justified in case of composite structures. These shortcomings can be appreciated in review papers [8] and [9].

In this work, we model the laminated composite structure as a double curved shell under static indentation and investigate the effect of curvature on the contact force distribution in the shell. Employing the Variational Asymptotic Theory(VAM)[10] we obtain a modified constitutive functional which takes into account the contact conditions prevailing on the contact surface intrinsically in the modeling process. The resulting theory is of the Reissner-Mindlin type but is geometrically exact. The shell deformable theory has three in-plane membrane strains, three out-of-plane curvature strains and two transverse shear strains as the unknowns. The modified functional contains an additional material force coupling term, taking into account the coupling between material properties, lay-up and thickness with the applied load. This is a new feature not accounted for in traditional 2-D Reissner-Mindlin shell solvers.

The non-linearity in contact analysis arises from the fact that the contact constraints are not known *a priori*. The contact forces are also not known and are solved from the multifreedom constraint formulation using Lagrangian technique. A hemispherical indentor is used to impart the specified indentation and simulation is done in view of rigid sphere contacting a flexible body. The indentor is represented using super-quadratics and an implicit description of the contact surface is obtained. Finite element analysis is done with 4-noded degenerate quadrilateral shell elements using Bernstein basis shape functions.

Variational Statement

A shell is a 3-D body with a relatively small thickness h and smooth reference surface, usually chosen to be the mid-surface (see Fig.1). The geometry of the reference surface can be mathematically represented by a set of arbitrary curvilinear coordinates, x_α. (Here and throughout the paper, Greek indices assume values 1 and 2 while Latin indices assume values 1,2 and 3. Dummy indices are summed over their entire range except where explicitly indicated). However, without loss of generality, the lines of curvatures are chosen to be the curvilinear coordinates to simplify the formulation. It is a natural and convenient choice to take the third coordinate x_3 normal to reference surface. We denote the composite shell as the *master* and the indentor as the *slave*. Excepting the

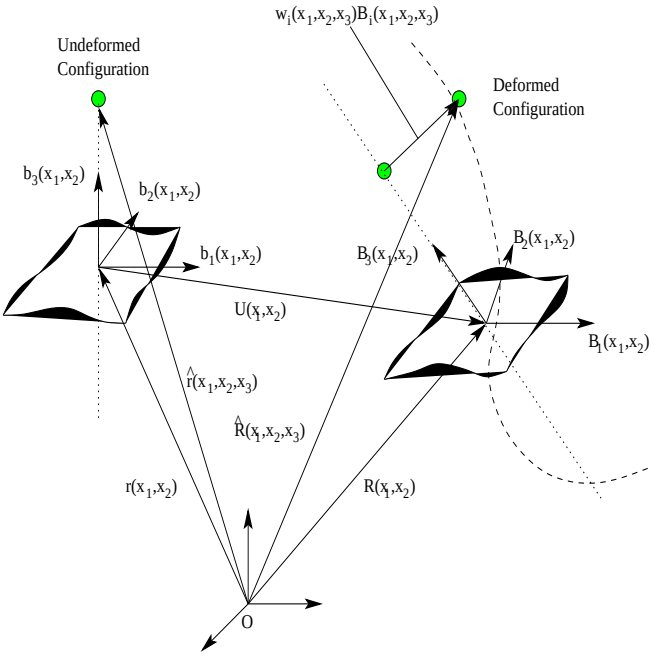

Figure 1. Schematic of shell deformation

variation of the warping field, all other variations are to be taken care of by the 2-D shell theory. The variation of the warping field is to be taken care of by VAM. Following the method in [10], we obtain the model for the 2-D Reissner-Mindlin composite shell. Where the indentor is in contact i.e. within the contact area $\Gamma_c \subset S$ we have the shell energy potential

$$\Pi_{\Re} = \frac{1}{2}\Re^T A_R \Re + \frac{1}{2}\gamma^T G \gamma + \Re^T F \tag{1}$$

whereas on $\Gamma_{\bar{c}} \subset S$, the portion of the shell outside the contact area we have

$$\Pi_{\Re} = \frac{1}{2}\Re^T A_R \Re + \frac{1}{2}\gamma^T G \gamma \tag{2}$$

where the generalized shell strain measures, $\Re$ and γ are given by

$$\Re = [\epsilon^*_{11}\ 2\epsilon^*_{12}\ \epsilon^*_{22}\ \kappa^*_{11}\ \kappa^*_{12}+\kappa^*_{21}\ \kappa^*_{22}\ ]^T \quad (3)$$

$$\gamma = [2\gamma_{13}\ 2\gamma_{23}\ ]^T \quad (4)$$

where $\epsilon_{\alpha\beta}$ are membrane strains, $\kappa_{\alpha\beta}$ are elastic curvatures and $\gamma_{\alpha 3}$ are transverse shear strains. However, the F-vector in Eqn.[1] represents the coupling between the unknown warping field and the unknown contact stresses t_N along x_3 direction. Since we are assuming normal contact, no in-plane forces act on the shell and as a result F-vector is a linear function of the contact traction t_N. Hence the A_R,G and F matrices can be generated for a unit load in the x_3 direction. This won't alter the nature of the problem since the A_R and G matrices do not depend on applied forces but rather on the material properties, ply lay-up and thickness. If $\overline{F}$ be the load-coupling vector for a **unit load** in the x_3 direction then we can write

$$F = t_N \overline{F} \quad (5)$$

Thus Eqn[1-2] are modified as

$$\Pi_{\Re} = \frac{1}{2}\Re^T A_R \Re + \frac{1}{2}\gamma^T G\gamma + \Re^T t_N \overline{F} \qquad \forall\ \ \Gamma \in \Gamma_c \quad (6)$$

$$\Pi_{\Re} = \frac{1}{2}\Re^T A_R \Re + \frac{1}{2}\gamma^T G\gamma \qquad \forall\ \ \Gamma \in \Gamma_{\overline{c}} \quad (7)$$

For the Reissner-Mindlin shell in local basis $\mathbf{b}_i$ the strain-displacement relations are given by

$$\epsilon^*_{\alpha\beta} = \frac{1}{2}([u]_{\alpha,\beta} + [u]_{\beta,\alpha}) \quad (8)$$

$$\gamma_{\alpha 3} = [w]_{,\alpha} - [\theta]_\alpha \quad (9)$$

whereas the curvatures are given by

$$\kappa^*_{\alpha\beta} = [\theta]_{\alpha,\beta} \quad (10)$$

The strain vector can then be written in terms of the unknowns as

$$\epsilon^* = \partial U \quad (11)$$

where

$$\partial = \begin{bmatrix} \frac{\partial}{\partial \underline{x}} & 0 & 0 & 0 & 0 \\ \frac{\partial}{\partial \underline{y}} & \frac{\partial}{\partial \underline{x}} & 0 & 0 & 0 \\ 0 & \frac{\partial}{\partial \underline{y}} & 0 & 0 & 0 \\ 0 & 0 & 0 & \frac{\partial}{\partial \underline{x}} & 0 \\ 0 & 0 & 0 & \frac{\partial}{\partial \underline{y}} & \frac{\partial}{\partial \underline{x}} \\ 0 & 0 & 0 & 0 & \frac{\partial}{\partial \underline{y}} \\ 0 & 0 & \frac{\partial}{\partial \underline{x}} & -1 & 0 \\ 0 & 0 & \frac{\partial}{\partial \underline{y}} & 0 & -1 \end{bmatrix}, U = \begin{Bmatrix} u \\ v \\ w \\ \theta_1 \\ \theta_2 \end{Bmatrix} \quad (12)$$

where the partial derivatives are expressed with respect to the lamina co-ordinate system ($\underline{x}$, $\underline{y}$, $\underline{z}$). Therefore, using Eqns.[6,7 & 11] and combining them we have

$$\Pi_{\Re} = \begin{cases} \frac{1}{2}\epsilon^{*T} A \epsilon^* + t_N[\epsilon_T \tilde{F} & \forall \quad \Gamma \in \Gamma_c \\ \frac{1}{2}\epsilon^{*T} A \epsilon^* & \forall \quad \Gamma \in \Gamma_{\overline{c}} \end{cases} \quad (13)$$

where

$$A = \begin{bmatrix} A_R & 0 \\ 0 & G \end{bmatrix}, \tilde{F} = \begin{Bmatrix} \overline{F} \\ 0 \\ 0 \end{Bmatrix} \quad (14)$$

The *master* displacement field is discretized as $U = N \cdot U_e$ where $N = \begin{bmatrix} \tilde{N}_1 & \tilde{N}_2 & \tilde{N}_3 & \tilde{N}_4 \end{bmatrix}$ and

$$\tilde{N}_i = \begin{bmatrix} N_i & 0 & 0 & 0 & 0 \\ 0 & N_i & 0 & 0 & 0 \\ 0 & 0 & N_i & 0 & 0 \\ 0 & 0 & 0 & N_i & 0 \\ 0 & 0 & 0 & 0 & N_i \end{bmatrix} \quad (15)$$

and contact force field as $t_N = \tilde{N}\bar{t}_N$ where $\tilde{N} = \begin{bmatrix} N_1 & N_2 & N_3 & N_4 \end{bmatrix}$. Over an element the functional can be written as

$$\Pi_{\Re} = \begin{cases} \frac{1}{2}U_e^T K_e U_e + U_e^T F_e \tilde{N}\bar{t}_N & \forall \quad \Gamma \subset \Gamma_c \\ \frac{1}{2}U_e^T K_e U_e & \forall \quad \Gamma \in \Gamma_{\overline{c}} \end{cases} \quad (16)$$

where

$$K_e = \int_{A_e} B^T A B dA_e \quad (17)$$

$$F_e = \int_{A_e} B^T \tilde{F} dA_e \quad (18)$$

and B is strain displacement matrix given by $B = \partial N$ of size $8 \times 5n$, n being the number of nodes.

If the entire *master* surface is discretized into n_e elements and if n_e^c elements come into contact then the functional for the entire surface can be written as

$$\Pi_{\Re} = \sum_{n_e} \frac{1}{2} U_e^T K_e U_e + \sum_{n_e^c} U_e^T F_e \tilde{N}\bar{t}_N \quad (19)$$

Contact Formulation

The contact constraints in the Lagrangian method are given by the following conditions:

$$t_N \leq 0 \quad (20)$$

$$g_N \geq 0 \quad (21)$$

$$t_N g_N = 0 \quad (22)$$

The above set of equations are the so called Kuhn-Tucker-Karaush conditions, where t_N is the contact traction and g_N is the gap function. Since we are considering the static indentation of the hemispherical impactor on the composite laminated shell, the kinetic energy of the indentor can be neglected. Moreover, the discretization of the indentor is also not necessary. Since the geometry of the rigid indentor is fixed once for all, the description of the surface normal at the contacting surface can be given in closed form at all points of contact. The gap function for the case of non-penetrability can be written according to [5] as:

$$g_N = w(x,y) - f(x,y) - h = 0 \quad (23)$$

where h is the indentation depth and $f(x,y)$ represents the indentor geometry in contact. Since we do not have any idea of the contact area *a priori*, the function $f(x,y)$ is not known until we perform a search of all the contact points that come into contact and satisfy the non-penetrability criteria. Assuming that an element is under contact at all the nodes, the contact contribution of a single element according to the Lagrange multiplier technique is given by

$$\Pi_e = t_N \cdot g_N \quad (24)$$

i.e.

$$\Pi_e = t_N \cdot (w(x_1,x_2) - f_e(x_1,x_2) - h_e) \quad (25)$$

or

$$\Pi_e = \tilde{N}\bar{t}_N \cdot (\underline{U} - \mathbf{f}_e - \mathbf{h}_e) \cdot \mathbf{n} \quad (26)$$

where

$$\underline{U} = \omega \cdot U,\ \mathbf{f}_e = \begin{Bmatrix} 0 \\ 0 \\ f_e(x,y) \end{Bmatrix},\ \mathbf{h}_e = \begin{Bmatrix} 0 \\ 0 \\ h_e \end{Bmatrix} \quad (27)$$

$$\text{with } \omega = \begin{bmatrix} 1 & 0 & 0 & 0 & 0 \\ 0 & 1 & 0 & 0 & 0 \\ 0 & 0 & 1 & 0 & 0 \end{bmatrix} \quad (28)$$

The description of the indentor surface coming into contact can be made with the use of the so-called *super-quadratics* functions[11] which for the hemispherical indentor become

$$f(x,y,z) = \left(\frac{x-x_0}{R}\right)^2 + \left(\frac{y-y_0}{R}\right)^2 + \left(\frac{z-z_0}{R}\right)^2 - 1 = 0 \quad (29)$$

The above explicit form is used for the contact detection phase. In the detection phase, each master node is checked if it comes into contact or not. The contact decision for a master node having coordinates (x_s,y_s,z_s) is governed by the following criteria[11]

$$\left(\frac{x_s-x_0}{R}\right)^2 + \left(\frac{y_s-y_0}{R}\right)^2 + \left(\frac{z_s-z_0}{R}\right)^2 - 1 \quad (30)$$

$$\leq 0 \Rightarrow \text{contact}$$

$$\left(\frac{x_s-x_0}{R}\right)^2 + \left(\frac{y_s-y_0}{R}\right)^2 + \left(\frac{z_s-z_0}{R}\right)^2 - 1 \quad (31)$$

$$> 0 \Rightarrow \text{no contact}$$

For the hemispherical contacting body, the direction of the surface normal at a particular location (x_1,x_2) on the *master* is given by

$$\mathbf{n} = \frac{grad(f)}{|grad(f)|} \quad (32)$$

Assuming that n_e^c elements come into contact, the contact energy is given by

$$\Pi_c = \sum_{n_e^c} \Pi_e \quad (33)$$

Using discretized master displacement field in Eqn.[27] and as a result in Eqn.[26] we have

$$\Pi_c = \sum_{n_e^c} \tilde{N}\bar{t}_N(\omega N U_e - \mathbf{f}_e - \mathbf{h}_e) \cdot \mathbf{n} \quad (34)$$

Element Formulation

We consider a typical shell element in Fig.[2] with the external faces curved while the sections across the thickness are generated by straight lines[12]. Pairs of points, i_{top} and i_{bottom} each with given Cartesian co-ordinates, prescribe the shape of the element.

Let (ξ,η) be the two curvilinear coordinates on the mid-surface of the shell and let ζ be the rectilinear

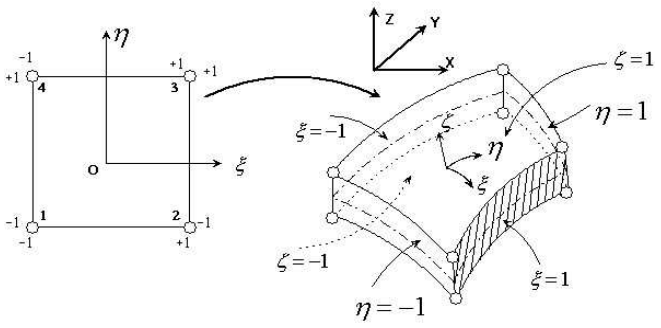

Figure 2. Iso-parametric and curved thick shell elements

coordinate in the thickness direction. Furthermore, we assume that ξ,η, and ζ vary between -1 and $+1$ on the respective faces of the element. Then in the paradigm of iso-parametric mapping, the *global* Cartesian co-ordinates of the shell mid-surface are related to the curvilinear co-ordinates by

$$\left\{ \begin{array}{c} x \\ y \\ z \end{array} \right\} = \sum_{i=1}^{n_e=4} N_i(\xi,\eta) \left[\left\{ \begin{array}{c} x_i \\ y_i \\ z_i \end{array} \right\} + \frac{1}{2} t_i \zeta \mathbf{v}_{3i} \right] \quad (35)$$

where

$$\mathbf{v}_{3i} = \frac{\mathbf{V}_{3i}}{\|\mathbf{V}_{3i}\|} = \left\{ \begin{array}{c} l_{3i} \\ m_{3i} \\ n_{3i} \end{array} \right\} \quad (36)$$

as the nodal vector is

$$\mathbf{V}_{3i} = \left\{ \begin{array}{c} x_i \\ y_i \\ z_i \end{array} \right\}_{top} - \left\{ \begin{array}{c} x_i \\ y_i \\ z_i \end{array} \right\}_{bottom} \quad (37)$$

The strains in the direction normal to the mid-surface are assumed to be negligible so that the displacement throughout the element is taken to be uniquely defined by the *three cartesian components* of the mid-surface node displacement and *two rotations* about two orthogonal directions normal to the nodal vector $\mathbf{V}_{3i}$. These two orthogonal directions are denoted by the unit vectors $\mathbf{v}_{1i}$ and $\mathbf{v}_{2i}$, with corresponding rotations θ_{1i} and θ_{2i}, so that the *global* displacement field can be specified in terms of curvilinear coordinates as

$$\left\{ \begin{array}{c} u \\ v \\ w \end{array} \right\} = \sum_{i=1}^{n_e=4} N_i(\xi,\eta) \left[\left\{ \begin{array}{c} u_i \\ v_i \\ w_i \end{array} \right\} + \frac{1}{2} t_i \zeta \mathbf{R}_i \left\{ \begin{array}{c} \theta_{1i} \\ \theta_{2i} \end{array} \right\} \right] \quad (38)$$

where

$$\mathbf{R}_i = \left[\begin{array}{cc} -\mathbf{v}_{2i} & \mathbf{v}_{1i} \end{array} \right] = \left[\begin{array}{cc} -l_{2i} & l_{1i} \\ -m_{2i} & m_{1i} \\ -n_{2i} & n_{1i} \end{array} \right] \quad (39)$$

Here $\mathbf{V}_{3i}$ is the vector to which a normal direction is to be constructed. The scheme for defining the vectors $\mathbf{v}_{1i}$ and $\mathbf{v}_{2i}$ is given by the flowchart in Fig.[3]. B is defined

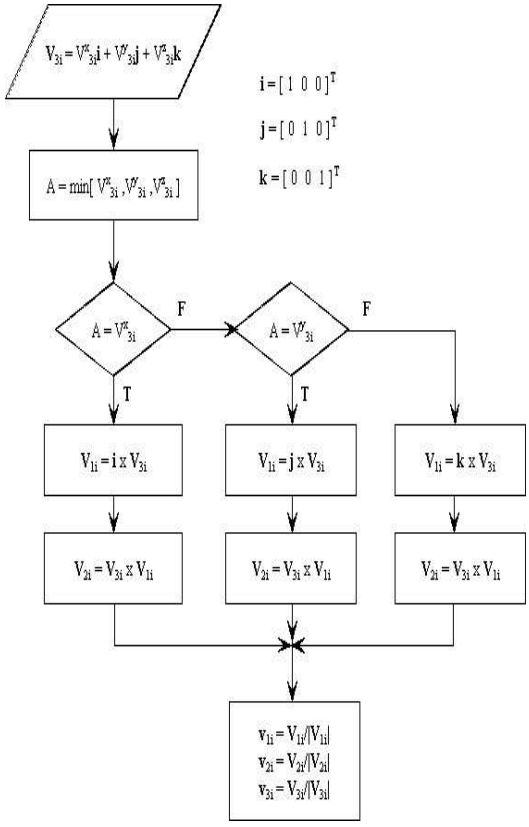

Figure 3. Flowchart for determining the orthogonal system of vectors given the normal vector $\mathbf{V}_3$

with respect to the local Cartesian coordinates ($\underline{x}$, $\underline{y}$, $\underline{z}$). Therefore, *two sets of transformations* are necessary before the element can be integrated with respect to the

curvilinear coordinates (ξ,η). First, the derivatives of the displacements related to the curvilinear co-ordinates, with respect to the global (x,y,z) co-ordinates is given by the inverse of the *Jacobian* as follows

$$\mathbf{\Gamma} = \mathbf{J}^{-1} = \begin{bmatrix} x,_\xi & y,_\xi \\ x,_\eta & y,_\eta \end{bmatrix}^{-1} = \frac{1}{|\mathbf{J}|}\begin{bmatrix} y,_\eta & -x,_\eta \\ -y,_\xi & x,_\xi \end{bmatrix} \quad (40)$$

where $|\mathbf{J}|$=($x,_\xi\, y,_\eta - x,_\eta\, y,_\xi$). A second transformation to the local Cartesian system ($\underline{x}$, $\underline{y}$, $\underline{z}$) will allow the strains and hence the strain-displacement matrix to be evaluated. The directions of the local axes are established from the vector normal to the $\xi - \eta$ mid-surface. This vector is found from the two vectors $\mathbf{x},_\xi$ and $\mathbf{x},_\eta$ which are tangential to the mid-surface. Thus,

$$\mathbf{V}_3 = \begin{bmatrix} x,_\xi \\ y,_\xi \\ z,_\xi \end{bmatrix} \times \begin{bmatrix} x,_\eta \\ y,_\eta \\ z,_\eta \end{bmatrix} = \begin{bmatrix} y,_\xi\, z,_\eta - y,_\eta\, z,_\xi \\ z,_\xi\, x,_\eta - z,_\eta\, x,_\xi \\ x,_\xi\, y,_\eta - x,_\eta\, y,_\xi \end{bmatrix} \quad (41)$$

The two orthogonal vectors $\mathbf{V}_1$ and $\mathbf{V}_2$ are constructed using the same procedure as given in Fig.[3]. The three orthogonal vectors are reduced to their unit magnitudes to obtain a matrix of unit vectors in the ($\underline{x}$, $\underline{y}$, $\underline{z}$) directions (which is in fact the direction cosine matrix) as

$$\mathbf{q} = [\mathbf{v}_1, \mathbf{v}_2, \mathbf{v}_3] \quad i.e. \quad \mathbf{q} = \begin{bmatrix} l_1 & l_2 & l_3 \\ m_1 & m_2 & m_3 \\ n_1 & n_2 & n_3 \end{bmatrix}^T \quad (42)$$

Using Eqns.[12,38] we have the strain-displacement matrix for a particular node i as

$$B^i = \begin{bmatrix} B_1^i & \mathbf{0} & B_2^i \\ \mathbf{0} & \mathbf{0} & B_1^i \\ \mathbf{0} & B_3^i & \end{bmatrix}_{8\times 5} \quad (43)$$

where the sub-matrices are defined as follows

$$\overline{B}_1^i = \begin{bmatrix} N_{i,\underline{x}} & 0 \\ N_{i,\underline{y}} & N_{i,\underline{x}} \\ 0 & N_{i,\underline{y}} \end{bmatrix} \quad (44)$$

$$\overline{B}_2^i = \frac{t_i}{2}\begin{bmatrix} (\zeta N_i),_{\underline{x}} & 0 \\ (\zeta N_i),_{\underline{y}} & (\zeta N_i),_{\underline{x}} \\ 0 & (\zeta N_i),_{\underline{y}} \end{bmatrix} \underline{\mathbf{R}}_i \quad (45)$$

and

$$\underline{\mathbf{R}}_i = \begin{bmatrix} -l_{2i} & l_{1i} \\ -m_{2i} & m_{1i} \end{bmatrix}$$

$$\overline{B}_3^i = \begin{bmatrix} N_{i,\underline{x}} & -1 - n_{2i}N_i & n_{1i}N_i \\ N_{i,\underline{y}} & -n_{2i}N_i & -1 + n_{1i}N_i \end{bmatrix} \quad (46)$$

The derivatives of the shape functions in the *local* Cartesian coordinate system from coordinate transformation is given as

$$\begin{Bmatrix} N_{i,\underline{x}} \\ N_{i,\underline{y}} \end{Bmatrix} = \underline{\mathbf{q}}\mathbf{J}^{-1}\begin{Bmatrix} N_{i,\xi} \\ N_{i,\eta} \end{Bmatrix} \quad (47)$$

where

$$\underline{\mathbf{q}} = \begin{bmatrix} l_1 & m_1 \\ l_2 & m_2 \end{bmatrix}, \ \underline{R}_i = \begin{bmatrix} -l_{2i} & l_{1i} \\ -m_{2i} & m_{1i} \end{bmatrix} \quad (48)$$

In our analysis, we are focussing on the middle surface of the shell. Hence $\zeta = 0$. Moreover, based on the assumption that the shell thickness is constant over all the nodes, we can write for the elements of the $\overline{B}_2^i$ matrix

$$(\zeta N_i),_{\underline{x}} = \frac{N_i n_1}{x,_\zeta} \quad (49)$$

$$(\zeta N_i),_{\underline{y}} = \frac{N_i n_2}{y,_\zeta} \quad (50)$$

and

$$x,_\zeta = \sum_{i=1}^{n_e=4} \frac{t_i}{2} N_i l_{3i} \quad (51)$$

$$y,_\zeta = \sum_{i=1}^{n_e=4} \frac{t_i}{2} N_i m_{3i} \quad (52)$$

The strain displacement matrix then takes the form

$$B = \begin{bmatrix} B^1 \mid B^2 \mid B^3 \mid B^4 \end{bmatrix}_{8\times 20} \quad (53)$$

Therefore the element stiffness matrix is obtained as

$$[K_e]_{20\times 20} = h\int_{-1}^{+1}\int_{-1}^{+1} B^T A B \, \|\mathbf{J}\| \, d\xi d\eta \quad (54)$$

Bernstein Basis Shape Functions

Theory of Bernstein polynomials is well developed and widely used in several areas of applied mathematics. It has been shown in [13] that the use of Bernstein polynomials for through the thickness approximations of displacements and stresses in the displacement-assumed

and mixed variational analysis of laminated composite plates provides uniquely accurate results.

Bernstein basis functions of degree N are defined as

$$B_n^N(t) = \frac{N!}{n!(N-n)!} t^n (1-t)^{N-n}; \qquad (55)$$

$$t \in [0,1]; \quad n = 0, 1, ..., N$$

where N may be any integer. For any value of n, Eqn.[55] defines the Nth degree polynomial. It is well-known that all algebraic polynomials of degree $\leq N$ constitute a linear space of dimension $N+1$. Since the $N+1$ functions $B_n^N(t)$, where $n = 0, 1, ..., N$ are linearly independent, they form a basis. Important properties of the Bernstein basis polynomials include extreme values at (0,1) i.e.,

$$B_n^N(0) = B_n^N(1) = \begin{cases} 0 & for\ n = 1, 2, ..., N-1 \\ 1 & for\ n = 0, N \end{cases} \qquad (56)$$

It satisfies symmetry as

$$B_n^N(t) = B_{N-n}^N(1-t) \qquad (57)$$

and positivity $B_n^N(t) \geq 0$. With Bernstein polynomials, we can design a 4-node quadratic element (i.e. $N = 3$) in Eqn.[55] and still get cubic displacement interpolation as well as slope continuity without the introduction of additional nodes. Considering that the Bernstein basis functions are applied in the (x_1,x_2) directions, we can write the basis functions for a **4-node quadrilateral iso-parametric element** as

$$X_n(\xi) = B_n^3(\xi) = \frac{3!}{n!(3-n)!} \xi^n (1-\xi)^{3-n} \qquad (58)$$

$$\forall \ \ \xi \in [0,1]$$

$$Y_n(\eta) = B_n^3(\eta) = \frac{3!}{n!(3-n)!} \eta^n (1-\eta)^{3-n} \qquad (59)$$

$$\forall \ \ \eta \in [0,1]$$

As can be seen, for the 4-node quadrilateral element we have 5 field variables namely u, v, w, θ_1 and θ_2 which implies that we have 20 d.o.f. per element. For comparison sake, if we were to use Lagrange family of elements with cubic approximations and 12-node quadrilateral iso-parametric element, we should have 60 d.o.f. per element compared to 20 d.o.f. in our case. Hence the current formulation leads to much more computationally efficient routines. Now each of the displacement approximations can be represented as

$$U_\alpha(\xi, \eta) = \sum_{f=1}^{F} U_f^\alpha N_f(\xi, \eta) \quad (\alpha = 1, 2, ..., 5) \qquad (60)$$

where

$$N_f(\xi, \eta) = N_{ij}(\xi, \eta) = B_i^3(\xi) B_j^3(\eta) \qquad (61)$$

$$f = j + 1 + 4i \qquad (62)$$

$$F = (3+1)(3+1) = 16 \qquad (63)$$

However, Bernstein basis functions provide the following properties to the functions $N_f(\xi,\eta)$

$$N_1(-1,-1) = 1 \qquad (64)$$

$$N_4(1,-1) = 1 \qquad (65)$$

$$N_{13}(1,1) = 1 \qquad (66)$$

$$N_{16}(-1,1) = 1 \qquad (67)$$

For the above four combinations of (i,j) all functions N_f except those listed in Eqns.[64-67] take zero values. Therefore, Bernstein functions can be viewed as special types of shape functions defining the 4-node iso-parametric quadrilateral element without edge, side or internal nodes. This element can have only 4-nodes regardless of the degree of Bernstein basis functions that is chosen to *approximate* the displacement field.

The iso-parametric shape functions for the 4-node element can then be written as

$$N_1 = \frac{1}{64}(1-\xi)^3(1-\eta)^3 \qquad (68)$$

$$N_2 = \frac{1}{64}(1+\xi)^3(1-\eta)^3 \qquad (69)$$

$$N_3 = \frac{1}{64}(1-\xi)^3(1+\eta)^3 \qquad (70)$$

$$N_4 = \frac{1}{64}(1+\xi)^3(1+\eta)^3 \qquad (71)$$

Solution of FE Equations

The total energy potential of any shell element in contact is now obtained from Eqn.[16 & 26] as

$$\Pi_T = \frac{1}{2} U_e^T K_e U_e + U_e^T F_e \tilde{N} \bar{t}_N$$

$$+ \tilde{N} \bar{t}_N \cdot (\omega N U_e - \mathbf{f}_e - \mathbf{h}_e) \cdot \mathbf{n} \qquad (72)$$

The Euler-Lagrange equations derived from the total functional are now given in matrix form as

$$\begin{bmatrix} K_{ee} & K_{ce} \\ K_{ce}^T & 0 \end{bmatrix} \begin{Bmatrix} U_e \\ \bar{t}_N \end{Bmatrix} = \begin{Bmatrix} 0 \\ R_c \end{Bmatrix} \qquad (73)$$

where

$$K_{ee} = K_e \quad (74)$$

$$K_{ce} = F_e\tilde{N} + (\omega N)^T \cdot \mathbf{n}\tilde{N} \quad (75)$$

$$R_c = \left[(\mathbf{f}_e + \mathbf{h}_e)^T \cdot \mathbf{n} \cdot \tilde{N}\right]^T \quad (76)$$

The submatrices defined in Eqn.[74-76] are assembled and after application of appropriate displacement boundary conditions and contact force constraints, the *augmented* Lagrangian stiffness matrix can be obtained as

$$\begin{bmatrix} K^a_{ee} & K^a_{ce} \\ K^{a\,T}_{ce} & 0 \end{bmatrix} \begin{bmatrix} \mathbf{U} \\ \mathbf{T} \end{bmatrix} = \begin{Bmatrix} 0 \\ \mathbf{R}_c \end{Bmatrix} \quad (77)$$

The above set of coupled equations in $\mathbf{U}$ and $\mathbf{T}$ can be solved to give the solution field as

$$\mathbf{T} = {K^a_{mod}}^{-1}\mathbf{R}_c \quad (78)$$

$$\mathbf{U} = -{K^a_{ee}}^{-1}K^a_{ce}K^{-1}_{mod}\mathbf{R}_c \quad (79)$$

$$where\ K_{mod} = -K^{a\,T}_{ce}{K^a_{ee}}^{-1}K^a_{ce} \quad (80)$$

The strains at the nodes are recovered through bilinear extrapolation using the bilinear shape functions from the computed strains at the Gaussian quadrature integration points.

Results and Discussion

A composite laminated shell model is considered to analyse the effects of curvature on the contact force within the purview of the static indentation process. We consider a composite laminated shell of *chord diameter* $2R_s = 50$mm, thickness $h = 3.8$mm and *radii of curvature* $R_1 = R_2 = 80.9$mm (i.e. having curvature $\kappa = 0.01236$rad/mm). The contacting body is a steel hemisphere of radius $R_{indt} = 12.7$mm. The geometric model is depicted in Fig. [4].

The radius of indentor being quite small compared to that of the shell, we can assume a normal contact. Moreover, the stiffness of steel is much larger that the transverse stiffness of the laminates. Therefore, the contact scenario can be thought of as a *rigid* body contacting the *flexible* composite shell. The indentor is assumed to be in contact with the shell reference/middle plane at the origin of the system of coordinates as shown in Fig. [5]. The shell top and bottom surface are also assumed to be indented equally.

The assumptions in the simulation can now be listed as follows:

- Thin shell model.

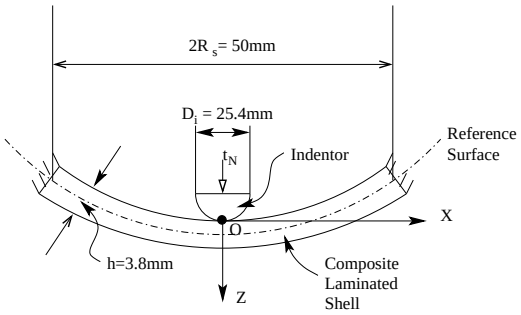

Figure 4. Geometry of the shell-indentor model

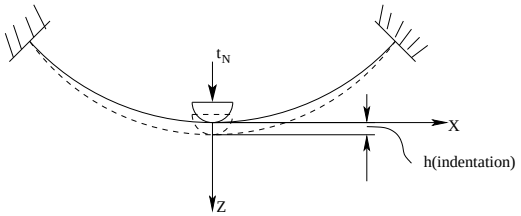

Figure 5. Simplified model for simulation of indentation

- Indentation is at the shell middle surface.
- Contact to be maintained at all stages.
- The top and bottom surfaces of the shell assume the same deformed profile of the middle surface upon indentation.
- The indentor is rigid.

The shell is clamped over the whole of the circumferance. The bottom surface is traction free and is allowed to curve upon indentation, while at the top surface normal tractions are present only within the region of contact. The 3-D shell reference surface is discretized with 4-node quadrilateral degenerate shell finite elements. Due to the symmetry of the structure, only a quarter of the model is taken for analysis to optimize on computational effort. The discretized shell reference surface is shown in 3-D in Fig. [6(a)] and the plan model is shown in Fig. [6(b)]. The discretization has 250 elements and 286 nodes. Assuming that the maximum contact area will stretch to a radius of the indentor, a heavier discretization is used upto a chord radius of 12.5mm from the center while the elements are sparse in the rest of the shell. Symmetric boundary conditions are imposed on the quarter-circle model along the perpedicular radial

lines. The indentor is placed in contact with the shell at

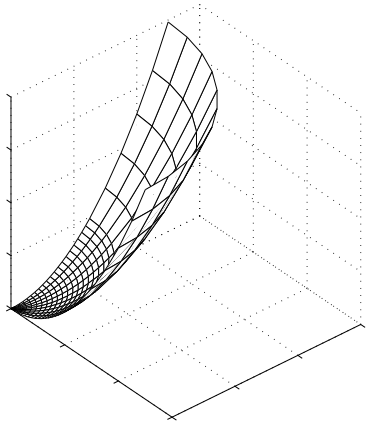

(a) 3−D Reference Surface Shell Model

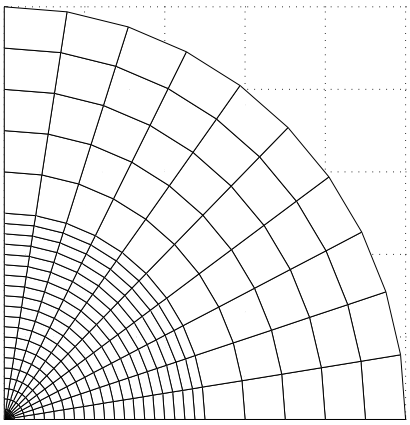

(b) Planar Discretized Shell Model

Figure 6. Finite element model

the origin O with zero indentation, Fig.[4]. The identation is carried out in steps of 0.1 mm from $h = 0$ mm to $h = 10$ mm. The material chosen for the shell is a Carbon/Epoxy laminate with mechanical properties as shown in Table[1]. The lay-up configurations chosen for the simulation are $[\theta/-\theta]_{2S}$ with $\theta = 0, 15, 30, ..., 90$. In addition, a cross ply configuration having a lay-up configuration of $[0/90]_{2S}$ is also simulated. Therefore three important cases are considered for simulation, namely

- Symmetric ply lay-up
- Cross ply lay-up
- Angle ply lay-up

Table 1
Mechanical Properties of *Carbon/Epoxy* Laminate

E_1 (GPa)	E_2 (GPa)	E_3 (GPa)
130.0	10.0	10.0
G_{12} (GPa)	G_{23} (GPa)	G_{13} (GPa)
6.0	6.0	3.0
ν_{12}	ν_{23}	ν_{13}
0.3	0.3	0.5

With the above mechanical properties, VAM was applied for obtaining the constitutive matrix and the force-material coupling matrix for different lay-ups that were considered. The contact area was determined at each indentation step and the resultant contact force T_N for given indentation depth was obtained. It was desired to obtain a power-law relationship of the form

$$T_N = C_1 h^{C_2} \tag{81}$$

between the contact force T_N and indentation depth h. C_1 and C_2 are coefficients which depend on lay-up configuration. Based on curve fitting technique, the coefficients C_1 and C_2 were obtained and are given in Table[2] for the different lay-ups that were considered. The fit curves

Table 2
C_1 and C_2 for different Lay-up Configurations

Lay-up Configuration	C_1	C_2
$(0/0)_{2S}$	327.9442	0.7021
$(15/-15)_{2S}$	390.0318	0.7128
$(30/-30)_{2S}$	481.8368	0.7286
$(45/-45)_{2S}$	555.2646	0.7130
$(60/-60)_{2S}$	582.3713	0.6987
$(75/-75)_{2S}$	602.1435	0.7043
$(90/-90)_{2S}$	564.8069	0.7019
$(0/90)_{2S}$	533.0893	0.7137

for three distinct cases of angle ply $[(45/-45)_{2S}]$, cross ply $[(0/90)_{2S}]$ and symmetric ply $[(30/-30)_{2S}]$ lay-ups are shown in Fig.[7]. The fit coeffiecients C_1 and C_2 for the symmetric lay-ups change with the lay-up angle θ and hence it was desired to obtain a functional relationship between these coefficients and θ. The fitting of C_1

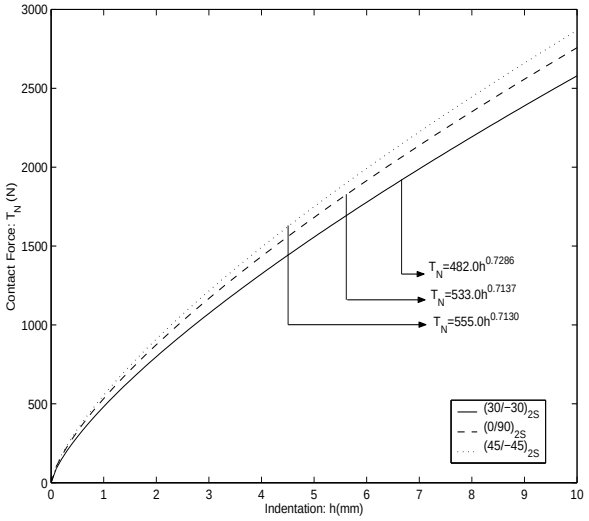

Figure 7. Contact Force relationship with Indentation Depth

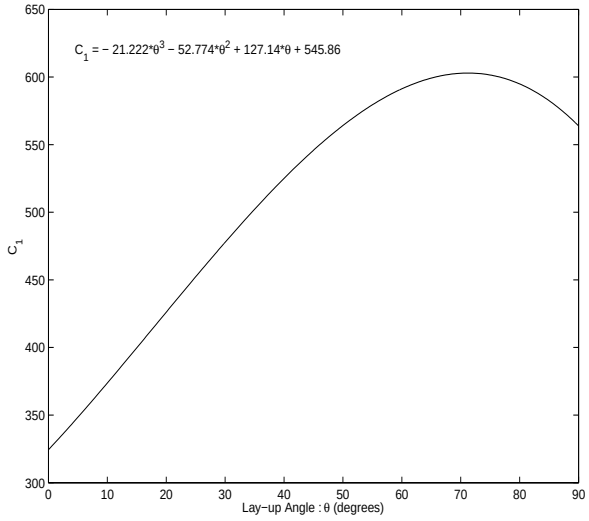

Figure 8. Variation of C_1 with lay-up angle θ

and C_2 values gives a best fit cubic polynomial in θ. The equations obtained are as follows

$$C_1 = -21.222\theta^3 - 52.774\theta^2 + 127.14\theta + 545.86 \quad (82)$$

$$C_2 = 0.011\theta^3 - 0.0063\theta^2 - 0.02\theta + 0.71 \quad (83)$$

The variation of C_1 and C_2 with θ is depicted in Fig.[8-9]. Therefore, from the above proceedings for symmetric lay-ups the following general contact power-law is proposed

$$T_N = C_1(\theta)h^{C_2(\theta)} \quad (84)$$

where the values of C_1 and C_2 can be obtained from Fig[8-9] for any arbitrary $(\theta/-\theta)_{2S}$ lay-up. One of the primary objectives of the study was to understand the effects of curvature of the shell model on the contact force arising out of indentation. In Fig.[10], the variations of contact force T_N with the curvature componenets κ_{11}, κ_{12}, and κ_{22} are shown. For the three different types of lay-ups that were considered, κ_{11} and κ_{22} tend to limit the contact force i.e. the change in contact force with increasing curvature, is reduced. If we consider κ_{11} and κ_{22}, there is a critical contact force for each of the lay-ups beyond which curvature effects become predominant and we start diverging from the plate model of analysis. This critical contact force is the point of inflection in the

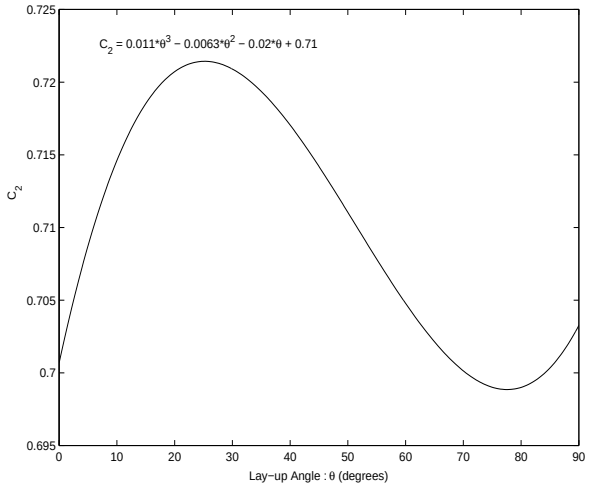

Figure 9. Variation of C_2 with lay-up angle θ

T_N vs κ_{11} and T_N vs κ_{22} curves. With indentation, the curvature components increase almost linearly as shown in Fig.[11]. The bending curvatures in the principal directions κ_{11} and κ_{22} vary considerably, while the twisting curvature κ_{12} shows little change for the *cross* ply lay-up. This is expected, because in cross ply lay-ups, there is no bending-twist coupling in the orthogonal principal directions. For the same reason, we find in Fig.[10] ap-

proximately infinite slope of the T_N vs κ_{12} curve for the cross-ply lay-up both at the onset and as the indentation is increased.

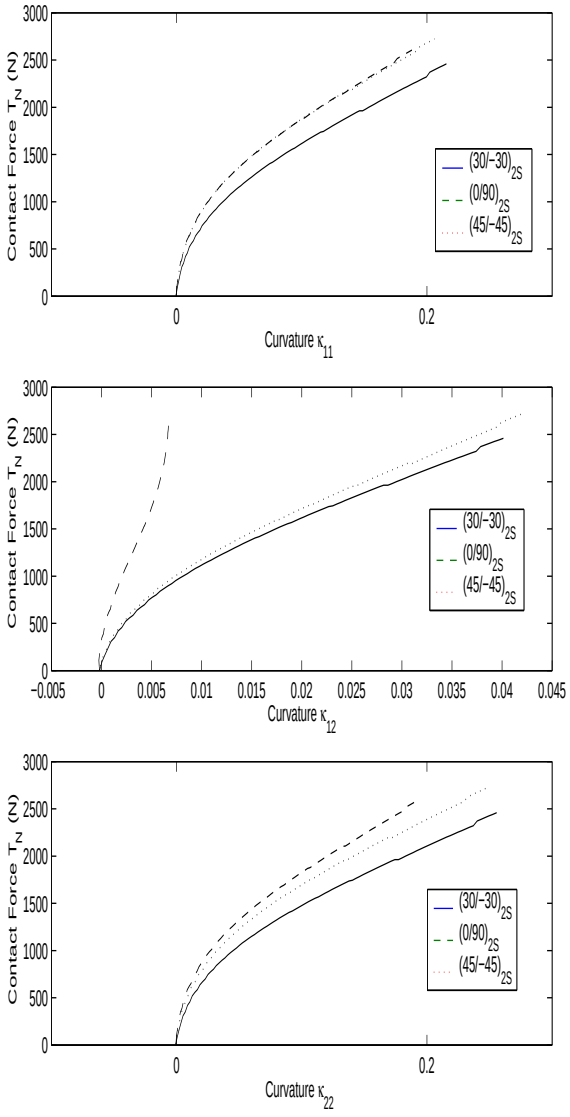

Figure 10. Effect of curvatures on contact force

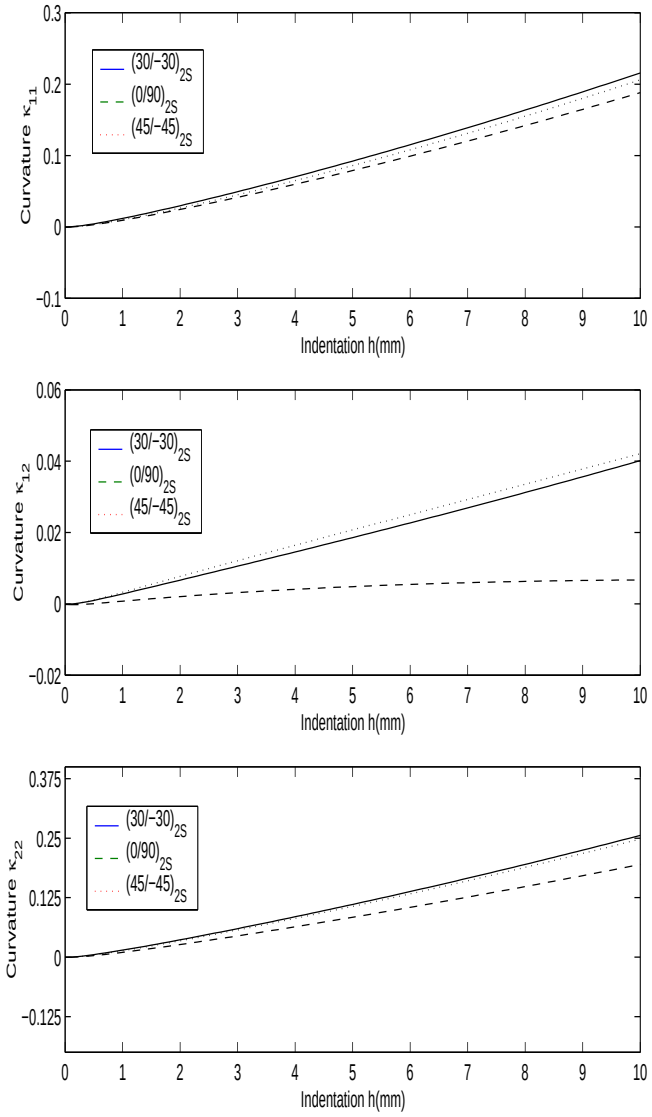

Figure 11. Variation of curvatures with indentation

The **energy** that is getting stored due to the indentation process, as contact force is developed, is a very important quantity. Especially in studies where the onset of delamination or damage is predicted by an energy criteria, the energy stored becomes all the more important. It can then be compared with the critical strain energy till the onset of delamination to predict the same. A polynomial curve-fitting is applied to get the variation of indentation energyof symmetric ply lay-ups with θ. A sixth order polynomial

$$E_{indt}(J) = 7.1\theta^6 + 61\theta^5 + 14\theta^4 - 250\theta^3 - 150\theta^2 + 330\theta + 350 \quad (85)$$

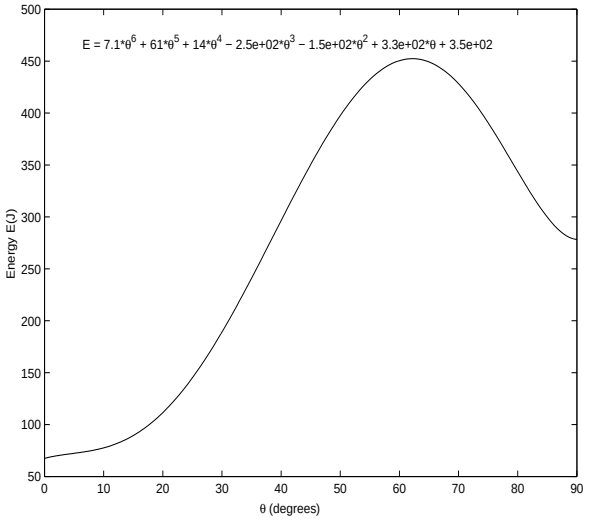

Figure 12. Variation of indentation energy with lay-up angle θ

is found to fit the data best. The variation shows that

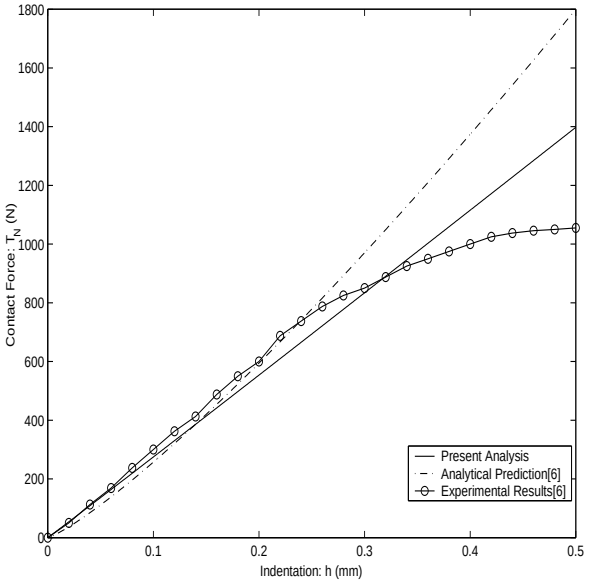

Figure 13. Comparison of contact force-indentation relationship between experimental results and present analysis for $(0_2/90_2/0_2/Adh\text{-}/110WF/Adh/0_2/90_2/0_2)$ lay-up sandwich laminate

for indentation from 0mm to 10mm, the $(60/-60)_{2S}$ lay-up configuration stores the maximum energy, and is most likely to undergo delamination/fracture when indented within the above-mentioned limits. The results of the simulation study were validated using the empirical relations and experimental results proposed by Anderson and Madenci[6] for sandwich laminated construction. A sandwich laminate with carbon epoxy face

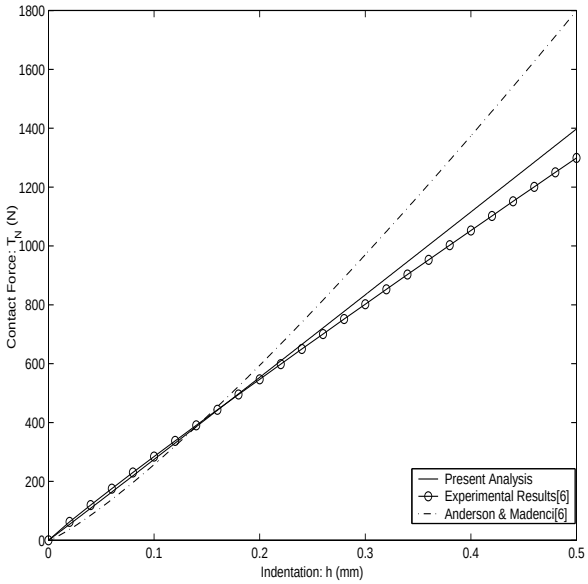

Figure 14. Comparison of contact force-indentation relationship between best-fit experimental results and present analysis for $(0_2/90_2/0_2/Adh\text{-}/110WF/Adh/0_2/90_2/0_2)$ lay-up sandwich laminate

sheets of lay-up $(0_2/90_2/90_2/0_2)$ bonded by an adhesive layer to $110WF$ foam core was considered. The measured contact force-indentation relationship for the panel configuration $(0_2/90_2/0_2/Adh/110WF/Adh/0_2/90_2/0_2)$ was taken. A mean value curve is chosen for the given results and the simulation results obtained are compared in Fig.[13]. The power law curve-fitting technique is applied to the experimental results and the same are also compared. The analytical expression proposed in [6] is also plotted for comparison purposes. The results obtained by the present analysis also are compared with the best-fit curve of the experimental results in Fig.[14].

Conclusion

The bending curvature brings about a non-linear variation of curvature with indentation. Moreover, while

investigating the contact force-indentation relationship for different ply angles, it was found that the fit coefficients for the power law relationship themselves depend on the lay-up angle. The coefficients turn out to be cubic polynomials in terms of the lay-up angle. The curvatures varied linearly with indentation while for no coupling between the orthogonal directions i.e. for the case of cross ply lay-up, the twist curvature remained virtually unaffected. Results compared with published experimental as well as analytical expressions for sandwich laminates showed better corelation with the experimental data, validating the efficacy of the current approach. The simulation results in this study had a correlation coefficient of 0.99974 with experimental data while published analytical form gave a correlation coefficient of 0.99644. So we can conclude that the present work predicts much more effectively the contact force variation compared to previous works, and is expected to mirror the real-life experimental data with much more accuracy. The expression for indentation energy, expected to be useful in delamination studies, was also provided.

REFERENCES

1. G. Caprino, V. Lopresto, The significance of indentation in the inspection of carbon fibre reinforced plastic panels damaged by low-velocity impact, Compos.Sci Technol 60 (2000) 1003–1012.
2. G. Caprino, V. Lopresto, Factors affecting the penetration energy of glass fiber reinforced plastics subjected to a concentrated transverse load, Proc. ECCM9, Brighton, UK, 4-7 June .
3. G. Caprino, V. Lopresto, On the penetration energy of fiber reinforced plastics under low-velocity impact conditions, Compos. Sci Technol 61 (2001) 65–73.
4. G. Caprino, A. Langella, V. Lopresto, Indentation and penetration of carbon fiber reinforced plastic laminates, Composites: Part B 34 319–325.
5. A. E. Bogdanovich, S. Yushanov, Three dimensional variational impact contact analysis of composite bars and plates, Composites: Part A 31 (2000) 795–814.
6. T. Anderson, E. Madenci, Graphite/epoxy foam sandwich panels under quasi-static indentation, Engineering Fracture Mechanics 67 (2000) 329–344.
7. D. H. Hodges, Contact stress from asymptotic reissner-mindlin plate theory, AIAA Journal 41 329–331.
8. A.K.Noor, M.Malik, An assessment of five modeling approaches for thermo-mechanical stress analysis of laminated composite panels, Computational Mechanics 25 (2000) 43–58.
9. A.K.Noor, S. W.Burton, Assessment of computational methods for multilayered composite shells, Applied Mechanics Review 43 (4).
10. W. Yu, D. H. Hodges, V. V. Volovoi, Asymptotic generalization of reissner-mindlin theory: accurate three-dimensional recovery for composite shells, Comput. Methods Appl. Mech. Engg 191 (2000) 5087–5109.
11. P. Wriggers, Computational Contact Mechanics, John Wiley & Sons, 2002.
12. O. Zienkiewicz, R. Taylor, The Finite Element Method, Vol. 2nd - Solid Mechanics, Butterworth & Heinemann, 2000.
13. A.E.Bogdanovich, C.M.Pastore, B.P.Deepak, A comparison of various 3-d approaches for the analysis of laminated composite structures, Composites Engrg. 5 (1995) 1105–1126.